

On Infusing Reachability-Based Safety Assurance within Probabilistic Planning Frameworks for Human-Robot Vehicle Interactions

Journal Title
XX(X):1–18
©The Author(s) 2019
Reprints and permission:
sagepub.co.uk/journalsPermissions.nav
DOI: 10.1177/ToBeAssigned
www.sagepub.com/



Karen Leung¹, Edward Schmerling¹, Mengxuan Zhang¹, Mo Chen², John Talbot¹, J. Christian Gerdes¹, and Marco Pavone¹

Abstract

Action anticipation, intent prediction, and proactive behavior are all desirable characteristics for autonomous driving policies in interactive scenarios. Paramount, however, is ensuring safety on the road—a key challenge in doing so is accounting for uncertainty in human driver actions without unduly impacting planner performance. This paper introduces a minimally-interventional safety controller operating within an autonomous vehicle control stack with the role of ensuring collision-free interaction with an externally controlled (e.g., human-driven) counterpart while respecting static obstacles such as a road boundary wall. We leverage reachability analysis to construct a real-time (100Hz) controller that serves the dual role of (i) tracking an input trajectory from a higher-level planning algorithm using model predictive control, and (ii) assuring safety by maintaining the availability of a collision-free escape maneuver as a persistent constraint regardless of whatever future actions the other car takes. A full-scale steer-by-wire platform is used to conduct traffic weaving experiments wherein two cars, initially side-by-side, must swap lanes in a limited amount of time and distance, emulating cars merging onto/off of a highway. We demonstrate that, with our control stack, the autonomous vehicle is able to avoid collision even when the other car defies the planner’s expectations and takes dangerous actions, either carelessly or with the intent to collide, and otherwise deviates minimally from the planned trajectory to the extent required to maintain safety.

Keywords

Probabilistic planning, safety-preserving controller, backward reachability analysis, vehicle model predictive control, human-robot interaction.

1 Introduction

Decision-making and control for mobile robots is typically stratified into levels. A high-level planner, informed by representative yet simplified dynamics of a robot and its environment, might be responsible for selecting an optimal, yet coarse trajectory plan, which is then implemented through a low-level controller that respects more accurate models of the robot’s dynamics and control constraints. While additional components may be required to flesh out a robot’s full control stack from model to motor commands, selecting the right “division of responsibilities” is fundamental to system design.

One consideration that defies clear classification, however, is how to ensure a mobile robot’s safety when operating in close proximity with a rapidly evolving and stochastic environment. Safety is a function of uncertainty in both the robot’s dynamics and those of its surroundings; high-level planners typically do not replan sufficiently rapidly to ensure split-second reactivity to threats, yet low-level controllers are typically too short-sighted to ensure safety beyond their local horizon.

Human-robot interactions are an unavoidable aspect of many modern robotic applications and ensuring safety for these interactions is critical, especially in applications such

as autonomous driving where collisions may lead to life-threatening injury. However, ensuring safety within the planning and control framework can be very challenging due to the uncertainty in how humans may behave. To quantify this uncertainty, robots often rely on generative models of human behavior in order to inform their planning algorithms ([Sadigh et al. 2016](#); [Schmerling et al. 2018](#)). This generally results in more efficient and communicative interactions since a robot can reason about the uncertainty to anticipate how a human may behave and leverage this to its advantage. In general, under nominal operating conditions that reflect the modeling assumptions, these model-based probabilistic planners can offer high performance (e.g., minimizing time and control effort for the robot). However, these planners alone are typically insufficient for ensuring absolute safety because (i) they depend on *probabilistic* models of human behavior and thus safety is not enforced deterministically, (ii) dangerous but low-likelihood events may not be adequately captured in the human behavior prediction model, and

¹Stanford University, Stanford, CA 94305, USA

²Simon Fraser University, Burnaby, BC V5A 1S6, Canada

Corresponding author:

Marco Pavone, 496 Lomita Mall, Rm. 261 Stanford, CA 94305

Email: pavone@stanford.edu

(iii) reasoning about these probabilistic behavior models is typically too computationally expensive for the planners to react in real time when humans strongly defy expectations and/or diverge from modeling assumptions.

In this work we implement a control stack for a full-scale autonomous car (the “robot”) engaging in close proximity interactions with a human-controlled vehicle (the “human”). Our control stack aims to stay true to planned trajectories from a high-level planner since freedom of motion is essential for the planner to carry out the driving task while conveying future intent to the other vehicle. At the same time, we allow the robot to deviate from the desired trajectory to the point that is necessary to maintain safety. Our primary tool for designing a controller that does not needlessly impinge upon the planner’s choices is *Hamilton-Jacobi (HJ) backward reachability*. We provide a brief overview of the reachability analysis literature relevant to our work in Section 3.

2 Related Work

For high-level planners, safety is often incentivized, but not strictly enforced as a hard constraint. For example, safety is often part of the objective function when selecting optimal plans, or represented via artificial potential fields (Wolf and Burdick 2008; Sadigh et al. 2016; Schmerling et al. 2018). Although these approaches are designed to account for interactive scenarios in which another sentient agent is a key environmental consideration, they contain competing objectives (i.e., collision avoidance vs. goal-oriented performance), often do not plan at a sufficiently high rate to account for rapidly-changing environments, and ultimately provide no theoretical framework for ensuring safety for both the human and the robot.

Another common approach to finding collision-free plans is to use *forward* reachability. The idea is to fix a time horizon and compute the set of states where the other agents could possibly be in the future and plan trajectories for the robot that avoid this set (Althoff and Dolan 2011; Liu et al. 2017; Lorenzetti et al. 2018). Although this gives a stronger sense of safety, this is only practical for short time horizons otherwise it will lead to overly conservative robot behaviors or even planning problem infeasibility as the set to avoid grows. In general, approaches that use forward reachability results in very conservative results, especially for interactive scenarios where freedom of motion (e.g., nudging) is necessary to convey intent. These methods, as well as methods that enforce safety as an objective, are often subjected to model simplification, such as using a linear dynamics model instead of a nonlinear one, or making simplifying assumptions for computational tractability. However, model simplifications can lead to overly conservative or imprecise results which may impede performance.

Safety can also be introduced at the low-level which often obeys higher fidelity dynamics models. A common approach in ensuring safe low-level controls is to use reactive collision avoidance techniques—the robot is normally allowed to apply any control, but switches to an avoidance controller when near safety violation. Examples of this general approach include HJ backward reachability-based

controllers which have been applied in such a switched fashion (Fisac et al. 2018; Chen and Tomlin 2018; Bajcsy et al. 2019) and have proven to be effective for avoiding other interacting agents and static obstacles. HJ reachability has been studied extensively and applied successfully in a variety of safety-critical interactive settings (Mitchell et al. 2005; Bokanowski et al. 2010; Gattami et al. 2011; Margellos and Lygeros 2011; Chen et al. 2017; Dhinakaran et al. 2017) due to its flexibility with respect to system dynamics, and its optimal (i.e., non-overly-conservative) avoidance maneuvers stemming from its equivalence to an exhaustive search over joint system dynamics. Other approaches include using a precomputed emergency maneuver library (Arora et al. 2015). A key drawback to switching controllers, however, is that the performance goals considered by the high-level planner are completely ignored when the reactive controller steps in. For some cases, this may be acceptable and necessary, but in general, it is desirable to ensure safety without unduly impacting planner performance where possible. Instead of switching to a different controller, Gray et al. (2013), Funke et al. (2017), and Brown et al. (2017) adapt the low-level online optimal controller to incorporate constraints that avoid static obstacles. The approach taken in Gray et al. (2013) aims to be minimally interventional, however, they only consider cases with disturbance uncertainty rather than environmental uncertainty stemming from the system interacting with other human agents. These approaches are able to strike the optimal balance between tracking performance and safety (i.e., optimizing performance subject to safety as a hard constraint), but these approaches as presented are effective for avoiding static obstacles only.

Inspired by the non-conservative nature and optimality of HJ reachability, and the performance of online optimal control for trajectory tracking, this work aims to infuse reachability-based safety assurance into the low-level controller such that when the robot is near safety violation, the robot is able to simultaneously maintain safety and follow the high-level plans without unduly impacting performance. To the best of our knowledge there has not been any work that explicitly addresses the integration of reachability-based safety controllers as a component within a robot’s control stack, i.e., with safety as a constraint upon a primary planning objective.

Statement of Contributions: The contributions of this paper are twofold. First, we propose a method for formally incorporating reachability-based safety within an existing optimization-based control framework. The main insight that enables our approach is the recognition that, near safety violation, the set of safety-preserving controls often contains more than just the optimal avoidance control. Instead of directly applying this optimal avoidance control when prompted by reachability considerations, as in a switching control approach, we quantify the set of safety-preserving controls and pass it to the broader control framework as a constraint. Our intent is to enable minimal intervention against the direction of a higher-level planner when evasive action is required. Second, we evaluate the benefits, performance, and trade-offs of this safe control methodology in the context of a probabilistic planning framework for the traffic weaving scenario studied at a

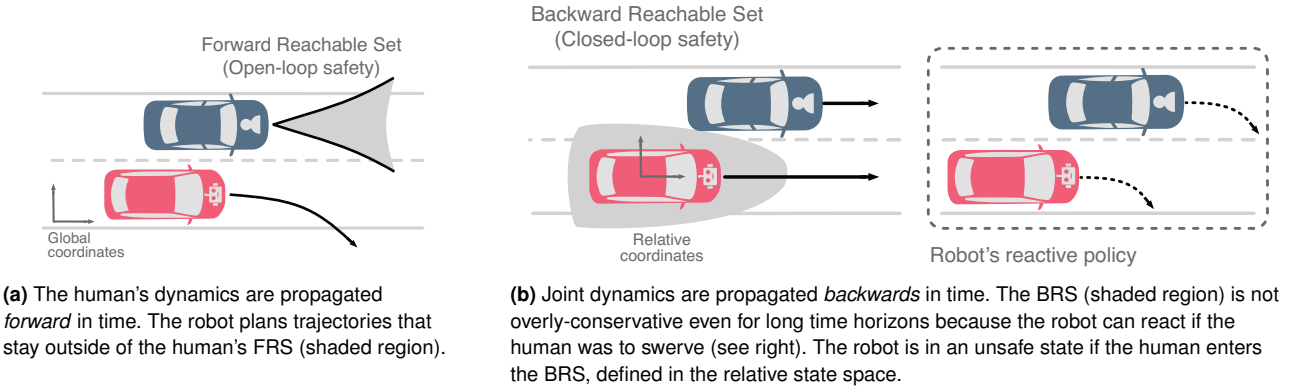


Figure 1. Illustration of forward and backward reachability, and how they are commonly used to ensure safe planning and controls. The robot and human are depicted in red and blue respectively.

high level in Schmerling et al. (2018), wherein two cars, initially side-by-side, must swap lanes in a limited amount of time and distance. Experiments with a full-scale steer-by-wire vehicle reveal that our combined control stack achieves better safety than applying a tracking controller alone to the planner output, and smoother operation (with similar safety) compared with a switching control scheme; in our discussion we provide a roadmap towards improving the level of safety assurance in the face of practical considerations such as unmodeled dynamics, as well as towards generalizations of the basic traffic weaving scenario.

A preliminary version of this work appeared at the 2018 International Symposium on Experimental Robotics (ISER). In this revised and extended version, we provide the following additional contributions: (i) an extension to the control framework to account for static obstacles, (ii) more exposition on the vehicle dynamics models used and a deeper discussion on the underlying modeling assumptions, (iii) an empirical study of the safety-efficiency trade-off for our approach, and (iv) additional experimental results including trials with a static road boundary wall.

3 Background: Hamilton-Jacobi Reachability

In this section, we provide a brief overview of reachability analysis as a tool for constructing safe trajectory plans, and introduce HJ backward reachability concepts relevant to this work.

3.1 Overview: Reachability Analysis

Given a dynamics model governing a robotic system incorporating control and disturbance inputs, reachability analysis is the study of the set of states that the system can reach from its initial conditions. It is often used for formal verification as it can give guarantees on whether or not the evolution of the system will be safe, i.e., whether the reachable set includes undesirable outcomes. Reachability analysis can be divided into two main paradigms: (i) forward reachability and (ii) backward reachability.

Forward Reachability Analysis: The *forward reachable set* (FRS) is the set of states that the system could

potentially be in after some time horizon t . This is computed by propagating the dynamics combined with all feasible control sequences and disturbances forward in time. When considering the interaction between two agents, for example a human and a robot, the forward reachable set is computed for the human and the robot plans to avoid this set to ensure collision-free trajectories (see Figure 1a). This *open-loop* mentality, however, leads to an overly-conservative robot outlook. That is, while considering actions in the present, the robot does not incorporate the possibility that its future observations of where the human goes might influence how much it actually needs to take avoidance actions; in short the robot's plan to avoid the FRS does not incorporate closed-loop feedback. To reduce the over-conservative nature of forward reachability, the time horizon t for which the FRS is computed over is typically kept small and is recomputed frequently. This approach has been found to be effective in finding collision-free trajectories (Althoff and Dolan 2014), but it is difficult to extend to interactive scenarios where there are more uncertainties in the rapidly changing environment. Aside from the overly-conservative nature of FRS, the key drawback with using forward reachability is that safety (i.e., avoiding the FRS) hinges on the planner's capabilities and operating frequency. Even if computing the FRS is instantaneous, the planner may still be unable to react to split-second threats.

Backward Reachability Analysis: Let the target set represent a set of undesirable states (e.g., collision states of the system). The *backward reachable set* (BRS) is the set of states that could result in the system being in the target set, assuming worst-case disturbances, after some time horizon t . Specifically, the BRS represents the set of states from which there does not exist a controller that can prevent the robot dynamics from being driven into the target set under worst-case disturbances within a time horizon t . As such, to rule out such an eventuality, the BRS is treated as the “*avoid set*”. Critical differences between the FRS and BRS are that (i) the BRS is computed *backwards* in time, and (ii) the BRS is computed assuming *closed-loop* reactions to the disturbances. Illustrated in Figure 1b, for the case of relative dynamics between human- and robot-controlled vehicles, computation of the BRS takes into account the fact that the robot is able to react to the human at any time and

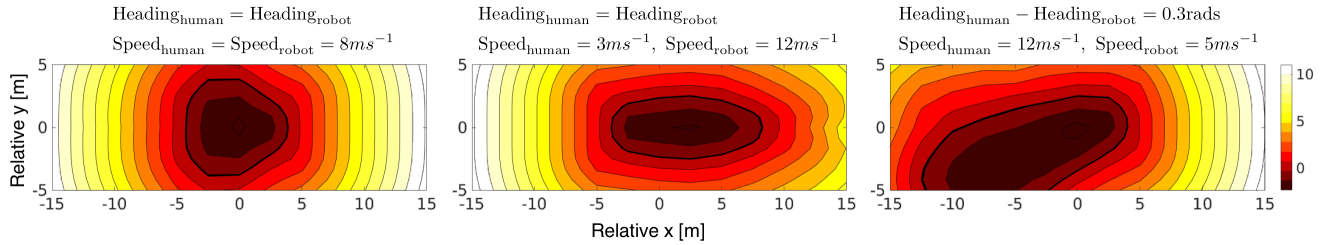


Figure 2. Contour plots of slices of the HJI value function V computed from the relative dynamics (see Equation (8)) and choice of signed distance as the terminal value function. Slices show V as a function of relative x and y position (see Figure 3 for an illustration of the human-robot relative pose) with all other states held fixed. The zero-level set, outlined with a thick black line, is the backwards reachable set from collision states (i.e., the avoid set).

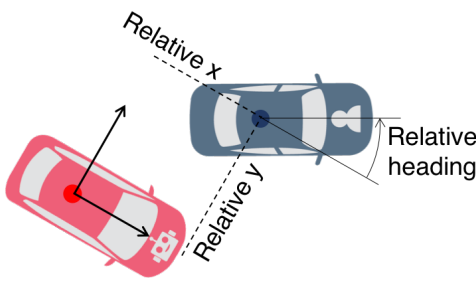


Figure 3. The relative human-robot coordinate frame and relative pose between the robot (red) car and human (blue) car. The frame is centered and rotated about the robot’s pose.

in any state configuration (if the human was to swerve into the robot, the robot can swerve too to avoid a collision). This leads to the BRS being less overly-conservative than the FRS. In practice, the results of the BRS computation are cached via a look-up table, and at run-time, the optimal robot policy can be computed via a near-instant lookup of the reachability cache. As such, we can always compute optimal actions for the robot at any state configuration and *regardless* of the high-level planner used.

We elect to use backward reachability because (i) its non-overly conservative nature stemming from the closed-loop computation ensures that safe controls will be used only when necessary and not unduly impact planner performance, (ii) safety is defined intrinsically in the BRS computation whereas safety using FRS-based approaches depends on whether the robot’s planned trajectory intersect the FRS, and (iii) it provides a computational handle on safe controls which can be evaluated at high operating frequencies to react to split-second threats.

Moreover, we will compute the BRS using Hamilton-Jacobi (HJ) reachability analysis, a particular approach to computing reachable sets. There are many existing approaches (Greenstreet and Mitchell 1998; Kurzhanski and Varaiya 2000; Frehse et al. 2011; Althoff and Krogh 2014; Majumdar et al. 2014), but there is always a trade-off between modeling assumptions, scalability, and representation fidelity (i.e., whether the method computes over- or under-approximations of the reachable set). Compared to alternatives approaches, HJ reachability is the most computationally expensive, but it is able to compute the BRS exactly* for any general nonlinear dynamics with

control and disturbance inputs because it essentially uses a brute force computation via dynamic programming. As a result, the BRS solution to the HJ reachability problem represents a constructive proof of the existence of a safety-preserving control policy (i.e., a safety certificate) from states outside the BRS. Despite the apparent computational drawbacks, we note that the BRS may be computed offline, and requires only a near-instant lookup during runtime, allowing it to be used in controllers or planners that run at a very high operational frequency.

3.2 Hamilton-Jacobi Backward Reachability Analysis

We briefly review relevant HJ backward reachability definitions for the remainder of this section; see Chen and Tomlin (2018) for a more in-depth treatment. HJ reachability casts the reachability problem as an optimal control problem and thus computing the reachable set is equivalent to solving the Hamilton-Jacobi-Isaacs (HJI) partial differential equation (PDE).

The general HJ reachability formulation is as follows. Let the system dynamics be given by $\dot{x} = f(x, u, d)$ where $x \in \mathbb{R}^n$ is the state, $u \in \mathcal{U} \subset \mathbb{R}^m$ is the control, and $d \in \mathcal{D} \subset \mathbb{R}^p$ is the disturbance. For example, x could be the state of a robot, u be the robot’s controls, d be environmental disturbances such as wind, and f be the dynamics of the robot. The system dynamics $f : \mathbb{R}^n \times \mathcal{U} \times \mathcal{D} \rightarrow \mathbb{R}^n$ are assumed to be uniformly continuous, bounded, and Lipschitz continuous in x for a fixed u and d . Let $\mathcal{T} \subseteq \mathbb{R}^n$ be the target set that the system wants to avoid at the end of a time horizon $|t|$ (note that $t < 0$ when propagating backwards in time). For collision avoidance, \mathcal{T} typically represents the set of states that are in collision with an obstacle. For brevity, the following description of HJ backward reachability will use notation relevant to the rest of the paper, that is, we are interested in collision avoidance for human-robot interactions. Despite the notation, the following theory is still applicable to general systems $\dot{x} = f(x, u, d)$ outside the domain of human-robot interactions.

In the context of human-robot interactions, $f(\cdot)$ describes the *relative dynamics* between the human and the robot (denoted by $f_{\text{rel}}(\cdot)$ where the subscript rel indicates the relative human-robot system), u corresponds to the robot’s

*With precision dependent on parameters of the numerical solver, e.g., discretization choices in mesh size/time step.

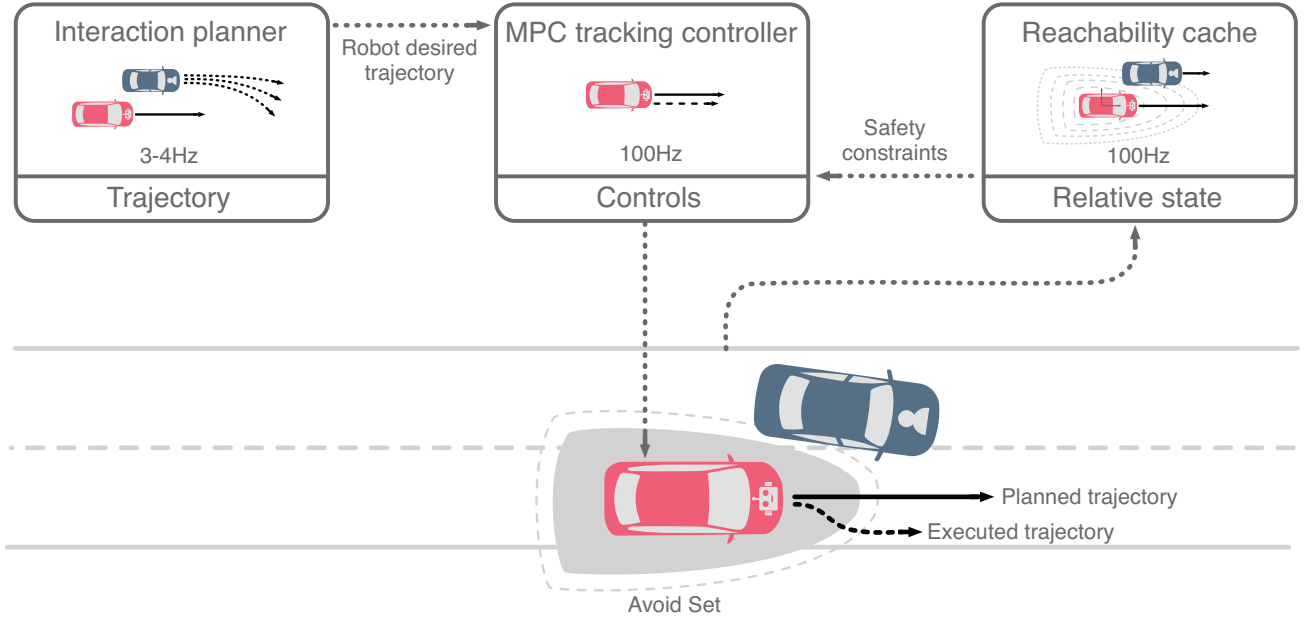


Figure 4. Decision-making and control stack for human-robot pairwise vehicle interactions. Our contribution in this work is the integration of safety-ensuring control constraints, derived from a HJ backward reachable set computed and cached offline, into a model predictive controller’s tracking optimization problem. A high-level interaction planner produces nominal trajectories for the robot car and the low-level safe tracking controller executes controls that minimally deviate from the planner’s choice if the vehicles approach the set of unsafe relative states.

controls, and d corresponds to the human’s controls since the human actions are treated as disturbance inputs. More concretely, let (x_R, u_R) represent the robot state and control, (x_H, u_H) represent the human state and control, and x_{rel} be the relative state between the human and the robot. Thus the relative dynamics of the robot and human are given by $\dot{x}_{\text{rel}} = f_{\text{rel}}(x_{\text{rel}}, u_R, u_H)$, and \mathcal{T} represents the set of relative states corresponding to when the human and robot are in collision. The formal definition of the BRS, denoted by $\mathcal{A}(t)$, for the human-robot relative system is

$$\begin{aligned} \mathcal{A}(t) := & \{\bar{x}_{\text{rel}} \in \mathbb{R}^n : \exists u_H(\cdot), \forall u_R(\cdot), \exists s \in [t, 0], \\ & x_{\text{rel}}(t) = \bar{x}_{\text{rel}} \wedge \dot{x}_{\text{rel}} = f_{\text{rel}}(x_{\text{rel}}, u_R, u_H) \wedge x_{\text{rel}}(s) \in \mathcal{T}\}. \end{aligned} \quad (1)$$

$\mathcal{A}(t)$ represents the set of “avoid states” at time t from which if the human followed an adversarial *policy* $u_H(\cdot)$, any robot *policy* $u_R(\cdot)$ would lead to the relative state trajectory $x_{\text{rel}}(\cdot)$ being inside \mathcal{T} within a time horizon $|t|$. Assuming optimal (i.e., adversarial) human actions, $\mathcal{A}(t)$ can be computed by defining a value function $V(t, x_{\text{rel}})$ which obeys the HJI PDE (Mitchell et al. 2005; Fisac et al. 2015); the solution $V(t, x_{\text{rel}})$ gives the BRS as its zero sublevel set:

$$\mathcal{A}(t) = \{x_{\text{rel}} : V(t, x_{\text{rel}}) \leq 0\}.$$

The HJI PDE is solved starting from the boundary condition $V(0, x_{\text{rel}})$, the sign of which reflects set membership of x_{rel} in \mathcal{T} .[†] Thus computing the BRS is equivalent to solving the HJI PDE with boundary condition $V(0, x_{\text{rel}})$; we cache the solution $V(t, x_{\text{rel}})$ to be used online as a look-up table.

For the case of the vehicle-vehicle interactions investigated in this work, when the control and maximum velocity capabilities of the human car are no greater than those of

the robot car, one can take the limit $t \rightarrow -\infty$ and obtain the infinite time horizon BRS \mathcal{A}_∞ with corresponding value function $V_\infty(x_{\text{rel}})$.[‡] Intuitively, this prescribed parity in control authority ensures that if the human and robot start sufficiently far apart, then the human will never be able to “catch” the robot. This holds even if the human car may have transient maneuverability advantages over the robot as we assume later in this work. That is, we expect that the BRS will not encompass the entire state space as $t \rightarrow -\infty$, and in practice we compute the BRS over a sufficiently large finite time horizon to the point where it appears that the BRS has converged. We recognize that we make a strong assumption on the human and robot’s control authority in enabling this computation. In reality, the human and robot car may have very different control authority (e.g., different engines resulting in different acceleration and velocity capabilities) and the infinite BRS may not be bounded. In such cases, practitioners may compute the BRS over a horizon suitable for the interaction where guarantees afforded by HJ reachability only hold over that time horizon. Illustrative slices of the value function and the BRS for the vehicle-vehicle relative dynamics with equal control and velocity capabilities considered in this work are shown in Figure 2 while Figure 3 illustrates the human-robot relative frame used to define the relative dynamics involved in the BRS computation (the mathematical details are given in Section 5.3). In Figure 2 (left), the pear-shaped BRS stems from the fact the robot car can swerve its front more rapidly than its rear to avoid collision. In Figure 2 (middle), if the robot

[†] See Section 8 for discussion of specific choices of $V(0, x_{\text{rel}})$.

[‡] For ease of notation going forward we will often write $V := V_\infty$.

car is traveling faster, it is unsafe for the robot car to be in the region behind the human car because a collision may be unavoidable if the human brakes abruptly. In Figure 2 (right), if the human car is traveling faster, in this case at an angle, it is unsafe for the robot to be in the region in front of the human car because the robot car may not be able to maneuver out of the way before the human catches up.

We can compute the optimal robot collision avoidance control

$$u_R^* = \arg \max_{u_R} \min_{u_H} \nabla V(x_{\text{rel}})^T f_{\text{rel}}(x_{\text{rel}}, u_R, u_H) \quad (2)$$

which offers the greatest increase in $V(x_{\text{rel}})$ assuming optimal (worst-case) actions by the human. Recall from Equation (1) that when the system is outside of the avoid set $\mathcal{A}(t)$ (i.e., $V > 0$), there exists a robot policy (e.g., Equation (2)) that keeps the robot safe over a time horizon $|t|$ regardless of any (including adversarial) policy taken by the human. Previous applications of HJI solutions switch to the optimal control (Equation (2)) when near the boundary of the BRS, i.e., when safety is nearly violated (Fisac et al. 2018; Bajcsy et al. 2019). This reflects the goal of HJ reachability-based safety is to ensure that the system stays outside of the avoid set $\mathcal{A}(t)$, that is, the value function should always stay positive.

In an interactive scenario where, for example, we may want to let a robot planner convey intent by nudging towards the human car to the extent that is safe, we prefer a less extreme control strategy. In the next section, we describe in detail how to infuse reachability-based safety assurance within a multi-tiered control framework that consists of different planning objectives.

4 Control Stack Architecture

In this section, we propose using a safety-preserving HJI controller, rather than switching to the optimal HJI controller defined in Equation (2), and describe how to incorporate it within an existing control stack—a high-level planner feeding desired trajectories to a low-level tracking controller—to enable safe human-robot interactions that minimally impinges on the high-level planning performance objective. The control stack architecture is illustrated in Figure 4. The proposed control stack is applicable to general human-robot interactions (e.g., an autonomous car interacting with a human-driven car, an autonomous manipulator arm working alongside a human, wheeled mobile robots navigating a crowded sidewalk). However, in this work, we focus on the traffic-weaving scenario, wherein two cars initially side-by-side must swap lanes in a limited amount of time and distance, because it is a representative interactive scenario that encapsulates many challenging characteristics inherent to human-robot interaction. Successful and smooth traffic-weaves rely on action anticipation, intent prediction, and proactive behavior from each vehicle, and ensuring safety is critical because collisions may lead to life-threatening injury.

4.1 Interaction Planner

Our proposed control framework is agnostic to the interaction planner used. The only assumption for the

planner is that it outputs desired trajectories (which presumably reflect high-performance goal-oriented nominal behavior) for the robot car to track. In general, high-level planners often optimize objectives that weigh safety considerations (e.g., distance between cars) relative to other concerns (e.g., control effort), and typical to human-robot interactive scenarios, they may reason anticipatively with respect to a *probabilistic* interaction dynamics model. That is, although the planner is encouraged to select safer plans, safety is not enforced as a deterministic constraint at the planning level.

In this work, we use the traffic-weaving interaction planner from Schmerling et al. (2018). It uses a predictive model of future human behavior to select desired trajectories for the robot car to follow, updated at $\sim 3\text{Hz}$. We extend this work by using a hindsight optimization policy (Yoon et al. 2008) instead of the limited-lookahead action policy in order to encourage more information-seeking actions from the robot.

4.2 MPC Tracking Controller

Given a desired trajectory from the interaction planner, the low-level tracking controller uses model predictive control (MPC) for computing optimal controls to track the desired trajectory. We assume that the outputs of the low-level tracking controller are used directly by the robot’s actuators (e.g., steering and longitudinal force commands for a vehicle, torque commands for each joint on a manipulator arm). As such, the MPC tracking controller typically uses a more accurate dynamics model and operates at a much higher frequency ($\sim 100\text{Hz}$) than the interaction planner. To ensure safety with respect to a dynamic obstacle (i.e., a human-driven vehicle) we incorporate additional constraints computed from HJ reachability analysis into the MPC problem. These constraints are designed to ensure that at each control step the robot car does not enter an unsafe set of relative states that may lead to collision.

For vehicle trajectory tracking, we adapt the real-time MPC tracking controller from Brown et al. (2017) by modifying it to include an additional invariant set constraint detailed in the next section. This MPC tracking controller, operating at 100Hz, computes optimal controls to track a desired trajectory by solving an optimization problem at each iteration. The optimization problem is based on a single track vehicle model (also known as the bicycle model) and incorporates friction and stability control constraints (in addition to control and state constraints) while minimizing a combination of tracking error and control derivatives. A more in-depth treatment of this combined MPC and HJI controller is given in Section 6.

4.3 Safety-Preserving HJI Control

Rather than switching to the optimal avoidance controller defined in Equation (2) when nearing safety violation, we propose adding containment in the *set of safety-preserving controls* as an additional constraint to the low-level MPC tracking controller. The set of safety-preserving controls

$$\mathcal{U}_R(x_{\text{rel}}) = \{u_R : \min_{u_H} \nabla V(x_{\text{rel}})^T f_{\text{rel}}(x_{\text{rel}}, u_R, u_H) \geq 0\} \quad (3)$$

represent the set of robot controls that ensure the value function is nondecreasing. This constraint can be computed online since the BRS is computed offline and the value function V and its gradient ∇V are cached. Online we employ a safety buffer $\epsilon > 0$ so that when the condition $V(x_{\text{rel}}) \leq \epsilon$ holds, indicating that the robot is nearing safety violation, we add the constraint $u_R \in \mathcal{U}_R(x_{\text{rel}})$ to the list of tracking controller constraints. By adding this additional safety-preserving constraint when near safety violation, the MPC tracking controller selects control actions that prevent the robot from further violating the safety threshold while simultaneously optimizing for tracking performance. This results in a *minimally interventional safety controller*—the MPC tracking controller will only minimally deviate from the desired trajectory to the extent necessary to maintain safety for the robot car.

For the traffic-weaving scenario investigated in this paper, the MPC problem for vehicle trajectory tracking (Brown et al. 2017) is formulated as a quadratic program (QP) (to enable fast solve time amenable to a 100Hz operating frequency) and hence requires the constraints to be linear. As such, we instead apply the constraint $u_R \in \tilde{\mathcal{U}}_R(x_{\text{rel}})$ where

$$\tilde{\mathcal{U}}_R(x_{\text{rel}}) = \{u_R : M_{\text{HJI}}^T u_R + b_{\text{HJI}} \geq 0\} \quad (4)$$

is a linearized approximation of $\mathcal{U}_R(x_{\text{rel}})$. Specifically, for the current relative state \tilde{x}_{rel} , current robot control \tilde{u}_R , and optimal, i.e., worst-case, human action defined analogously to Equation (2) u_H^* , the terms in the linearization are

$$M_{\text{HJI}} = \frac{\partial}{\partial u_R} (\nabla V^T f_{\text{rel}}(x_{\text{rel}}, u_R, u_H)) \Big|_{(\tilde{x}_{\text{rel}}, u_H^*, \tilde{u}_R)}$$

$$b_{\text{HJI}} = \nabla V^T f_{\text{rel}}(\tilde{x}_{\text{rel}}, u_H^*, \tilde{u}_R) - M_{\text{HJI}}^T \tilde{u}_R.$$

In general, $\mathcal{U}_R(x_{\text{rel}})$ may not be a half-space, leading to the linear approximation $\tilde{\mathcal{U}}_R(x_{\text{rel}})$ including controls outside of $\mathcal{U}_R(x_{\text{rel}})$. However, since we bound the change in the control inputs across each time step, feasible controls remain close to the linearization point where the approximation error is small.

5 Dynamics

In this section, we detail the vehicle dynamics model used to model the robot and human car, the relative dynamics model between the human and the robot necessary for computing the BRS, and the tracking dynamics used for the MPC tracking controller. We use a six-state nonlinear single track model to describe the robot car’s dynamics and assume the human car obeys a four-state dynamically extended nonlinear unicycle model with longitudinal acceleration and yaw rate as control inputs. As a result, the relative dynamics model has seven states. This represents a compromise between model fidelity and the number of state dimensions in the relative dynamics; increasing the former reduces the amount of model mismatch with the real system while reducing the latter is essential since solving the HJI PDE suffers greatly from the curse of dimensionality. The computation becomes notoriously expensive past five or more state dimensions without compromising on grid discretization or employing some decoupling strategy.

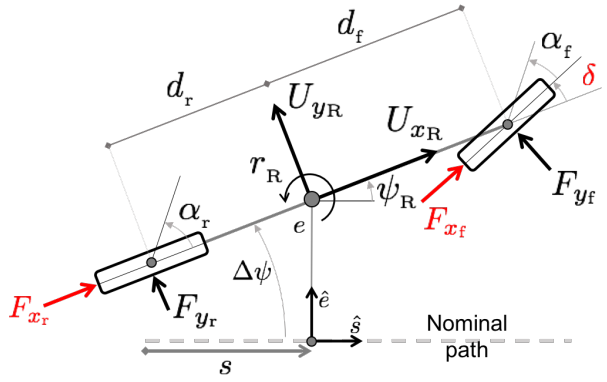


Figure 5. Schematic of the single track model (bicycle model) tracking a path. This is the dynamics model used to describe the robot vehicle.

5.1 Robot Vehicle Dynamics

The robot car (denoted by subscript R) will be modeled using the single track vehicle model illustrated in Figure 5. Let (p_{x_R}, p_{y_R}) be the position of the robot car’s center of mass defined in an inertial reference frame and ψ_R be the yaw angle (heading) of the robot car relative to the horizontal axis. U_{x_R} and U_{y_R} are the velocities in the robot car’s body frame, and r_R is the yaw rate. The state for the single track model is $x_R = [p_{x_R} \ p_{y_R} \ \psi_R \ U_{x_R} \ U_{y_R} \ r_R]^T$. The control input $u_R = [\delta \ F_x]^T$ consists of the steering command δ and longitudinal tire force F_x which is distributed between the front and rear tires $F_x = F_{x_f} + F_{x_r}$ via a fixed mapping. Assuming a quadratic model of longitudinal drag force ($F_{x_{\text{drag}}} = -C_{d_0} - C_{d_1} U_{x_R} - C_{d_2} U_{x_R}^2$) and for vehicle mass (m) and moment of inertia (I_{zz}), and the distances from the center of mass to the front and rear axles (d_f, d_r), the equations of motion for the robot car are

$$\dot{x}_R = \begin{bmatrix} U_{x_R} \cos \psi_R - U_{y_R} \sin \psi_R \\ U_{x_R} \sin \psi_R + U_{y_R} \cos \psi_R \\ r \\ \frac{1}{m}(F_{x_f} \cos \delta - F_{y_f} \sin \delta + F_{x_r} + F_{x_{\text{drag}}}) + r_R U_{y_R} \\ \frac{1}{m}(F_{y_f} \cos \delta + F_{y_r} + F_{x_f} \sin \delta) - r_R U_{x_R} \\ \frac{1}{I_{zz}}(d_f F_{y_f} \cos \delta + d_r F_{x_f} \sin \delta - d_r F_{y_r}) \end{bmatrix} \quad (5)$$

The controls are assumed to be limited by the steering system, friction limits, and power capacity of the vehicle. Using the brush coupled tire model by Pacejka (2002), the lateral tire force F_{y_i} and F_{z_i} at the front and rear tires is a function of slip angle (α_f, α_r), tire cornering stiffness ($C_{\alpha_f}, C_{\alpha_r}$), longitudinal tire forces (F_{x_f}, F_{x_r}), coefficient of friction (μ), and normal tire forces (F_{x_f}, F_{z_r}). As such, the lateral tire force for either the front or rear tires (denoted by $i \in \{f, r\}$) is

$$F_{y_i} = \begin{cases} 0 & \text{if } F_{x_i} > \mu F_{z_i} \\ -C_{\alpha_i} \tan \alpha_i (1 - \gamma + \frac{1}{3}\gamma^2) & \text{if } \gamma < 1 \\ -F_{y_{\max}} \text{sign}(\tan \alpha_i) & \text{if } \gamma \geq 1 \end{cases} \quad (6)$$

where $\gamma = \left| \frac{C_{\alpha_i} \tan \alpha_i}{3F_{y_{\max}}} \right|$ and $F_{y_{\max}} = \sqrt{\mu^2 F_{z_i}^2 - F_{x_i}^2}$. The slip angles and normal forces (accounting for weight transfer

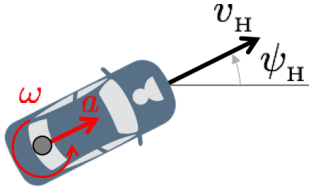


Figure 6. Schematic of the dynamically-extended unicycle model. This is the dynamics model used to describe the human vehicle.

due to F_{x_i}) for the front and rear tires can be computed using the following equations

$$\begin{aligned}\alpha_f &= \tan^{-1} \frac{U_{yR} + d_f r_R}{U_{xR}} - \delta, & \alpha_r &= \tan^{-1} \frac{U_{yR} - d_r r_R}{U_{xR}}, \\ F_{z_f} &= \frac{mgd_r - h\tilde{F}_x}{L}, & F_{z_r} &= \frac{mgd_f + h\tilde{F}_x}{L},\end{aligned}$$

where h is the distance from the center of mass to the ground and $\tilde{F}_x = F_{x_f} \cos \delta - F_{y_f} \sin \delta + F_{x_r}$ is the total longitudinal force in the vehicle's body frame.

5.2 Human Vehicle Dynamics

The human car (denoted by subscript H) will be modeled using the dynamically extended unicycle model illustrated in Figure 6. Let (p_{xH}, p_{yH}) be the position of the center of the human car's rear axle defined in an inertial reference frame and ψ_H be the yaw angle (heading) of the human car relative to the horizontal axis. The velocity of the human car in the vehicle frame is v_H . The state for the dynamically extended unicycle model is $x_H = [p_{xH} \ p_{yH} \ \psi_H \ v_H]^T$. The control input $u_H = [\omega \ a]^T$ consists of the yaw rate ω and longitudinal acceleration a . The control limits of the human car are chosen such that the robot and human car share the same power, steering, and friction limits. The equations of motion for the human car are

$$\dot{x}_H = \begin{bmatrix} v_H \cos \psi_H \\ v_H \sin \psi_H \\ \omega \\ a \end{bmatrix}. \quad (7)$$

Due to its simpler dynamics representation, the human car has a transient advantage in control authority over the robot car (it may change its path curvature discontinuously, while the robot may not), but by equating the steady-state control limits we ensure that the infinite time horizon BRS computation converges.

5.3 Relative Dynamics

The relative state (denoted by subscript rel) between the robot car and human car is defined with respect to a coordinate system centered on and aligned with the robot car's vehicle frame. We define the relative position $(p_{x_{\text{rel}}}, p_{y_{\text{rel}}})$ as

$$\begin{bmatrix} p_{x_{\text{rel}}} \\ p_{y_{\text{rel}}} \end{bmatrix} = \begin{bmatrix} \cos \psi_R & \sin \psi_R \\ -\sin \psi_R & \cos \psi_R \end{bmatrix} \begin{bmatrix} p_{xH} - p_{xR} \\ p_{yH} - p_{yR} \end{bmatrix},$$

and the relative heading ψ_{rel} as $\psi_{\text{rel}} = \psi_H - \psi_R$.

Since the velocity states are defined with respect to the vehicle frame, we cannot define analogous relative velocity states and must include the individual velocity states of each vehicle. As such, the relative state for the human-robot vehicle system is $x_{\text{rel}} = [p_{x_{\text{rel}}} \ p_{y_{\text{rel}}} \ \psi_{\text{rel}} \ U_{xR} \ U_{yR} \ v_H \ r_R]^T$. In the language of HJ reachability, the disturbance input of the system is the human car's control $d = u_H = [\omega \ a]^T$ and the control input is the robot car's control $u = u_R = [\delta \ F_x]^T$. Combining Equations (5) and (7), the equations of motion for the relative system are

$$\dot{x}_{\text{rel}} = \begin{bmatrix} v_H \cos \psi_{\text{rel}} - U_{xR} + p_{y_{\text{rel}}} r_R \\ v_H \sin \psi_{\text{rel}} - U_{yR} - p_{x_{\text{rel}}} r_R \\ \omega - r_R \\ \frac{1}{m}(F_{x_f} \cos \delta - F_{y_f} \sin \delta + F_{x_r} + F_{x_{\text{drag}}}) + r_R U_{yR} \\ \frac{1}{m}(F_{y_f} \cos \delta + F_{y_r} + F_{x_f} \sin \delta) - r_R U_{xR} \\ a \\ \frac{1}{I_{zz}}(d_f F_{y_f} \cos \delta + d_f F_{x_f} \sin \delta - d_r F_{y_r}) \end{bmatrix}. \quad (8)$$

5.4 Tracking Dynamics

The tracking MPC controller relies on an error dynamics model. Define a path (see Figure 5) through space where s is the distance along the path and at any distance s , we know the path heading $\psi(s)$, the curvature $\kappa(s)$, and a coordinate system (\hat{s}, \hat{e}) tangential and normal to the path. Given the position and heading of the robot car, we can project the car to the closest point on the path. Let the lateral error e be the lateral distance along direction \hat{e} and $\Delta\psi = \psi_R - \psi_{\text{path}}$ be the robot car's heading relative to the path computed from this closest point. Using this projection and the robot car's dynamics from Equation (5), we can compute the error dynamics relative to the desired path. Using the same notation defined previously in Equation (5), the state for the robot car tracking a desired path is $\hat{x} = [s \ U_{xR} \ U_{yR} \ r_R \ \Delta\psi \ e]^T$ and the controls $u = u_R = [\delta \ F_x]^T$. The tracking dynamics are

$$\dot{\hat{x}} = \begin{bmatrix} U_{xR} \cos \Delta\psi - U_{yR} \sin \Delta\psi \\ \frac{1}{m}(F_{x_f} \cos \delta - F_{y_f} \sin \delta + F_{x_r} + F_{x_d}) + r_R U_{yR} \\ \frac{1}{m}(F_{y_f} \cos \delta + F_{y_r} + F_{x_f} \sin \delta) - r_R U_{xR} \\ \frac{1}{I_{zz}}(d_f F_{y_f} \cos \delta + d_f F_{x_f} \sin \delta - d_r F_{y_r}) \\ r - (U_{xR} \cos \Delta\psi - U_{yR} \sin \Delta\psi) \kappa(s) \\ U_{xR} \sin \Delta\psi + U_{yR} \cos \Delta\psi \end{bmatrix}. \quad (9)$$

6 The MPC+HJI Trajectory Tracking Controller

In this section, we detail the optimization problem used in the MPC+HJI tracking controller, describe how this problem can be adapted to accommodate collision avoidance for static obstacles, and provide numerical details about the BRS computation used in this formulation. Central to an MPC controller is an optimization problem; at each time step, the controller solves an optimization problem to find an optimal

control sequence, passes the first control input to the actuator, and then repeats this process. To be amenable to real-time applications, the optimization problem requires a fast solve time (~ 0.01 s). In this work, the MPC tracking problem is formulated as a convex optimization problem, namely a QP, enabling the use of efficient solvers (Mattingley and Boyd 2012; Stellato et al. 2017) which are capable of solving the QP within the tight operating frequency.

6.1 Optimization Problem

Both the trajectory tracking objective and safety-preserving control constraint rely on optimizing over the robot steering and longitudinal force inputs simultaneously. Let $q_k = [\Delta s_k \ U_{xR,k} \ U_{yR,k} \ r_{R,k} \ \Delta\psi_k \ e_k]^T$ be the state of the robot car with respect to a nominal trajectory at discrete time step k . Δs_k , e_k and $\Delta\psi_k$ denote longitudinal, lateral, and heading error; $U_{xR,k}$, $U_{yR,k}$, and $r_{R,k}$ are body-frame longitudinal and lateral velocity, and yaw rate respectively as defined in Figure 5. Let $u_k = [\delta_k \ F_{x,k}]^T$ be the controls at step k and let $A_k q_k + B_k^- u_k + B_k^+ u_{k+1} + c_k = q_{k+1}$ denote linearized first-order-hold dynamics of Equation (9). We adopt the varying time steps method and stable handling envelope constraint from Brown et al. (2017). To ensure the existence of a feasible solution, we use slack variables $\sigma_{\beta,k}$, $\sigma_{r,k}$, and $\sigma_{HJI,k}$ on the stability and HJI constraints. The HJI reachability constraint $M_{HJI} u_k + b_{HJI} \geq -\sigma_{HJI}$ is activated only when $V(x_{rel}) \leq \epsilon$. Although HJI theory suggests that applying this constraint on the next action alone is sufficient, we apply it over the next $N_{HJI} = 3$ timesteps (30ms lookahead) to account for the approximations inherent in our QP formulation. The MPC tracking problem is a quadratic program of the form

$$\begin{aligned} & \underset{q, u, \sigma, \sigma_{HJI}, \Delta\delta, \Delta F_x}{\text{minimize}} \sum_{k=1}^T \Delta s_k^T Q_{\Delta s} \Delta s_k + \Delta\psi_k^T Q_{\Delta\psi} \Delta\psi_k + \\ & \quad e_k^T Q_e e_k + \Delta\delta_k^T R_{\Delta\delta} \Delta\delta_k + \\ & \quad \Delta F_{x,k}^T R_{\Delta F_x} \Delta F_{x,k} + \\ & \quad W_\beta \sigma_{\beta,k} + W_r \sigma_{r,k} + W_{HJI} \sigma_{HJI,k} \\ & \text{subject to } q_1 = q_{curr}, \quad u_1 = u_{curr}, \\ & \quad \delta_{k+1} - \delta_k = \Delta\delta_k, \\ & \quad \Delta\delta_{\min} \leq \Delta\delta_k \leq \Delta\delta_{\max}, \\ & \quad \delta_{\min} \leq \delta_k \leq \delta_{\max}, \\ & \quad F_{x,k+1} - F_{x,k} = \Delta F_{x,k}, \\ & \quad F_{x,\min} \leq F_{x,k} \leq F_{x,\max}, \\ & \quad U_{x,\min} \leq U_{xR,k} \leq U_{x,\max}, \\ & \quad \sigma_{\beta,k} \geq 0, \quad \sigma_{r,k} \geq 0, \\ & \quad \sigma_{HJI,j} \geq 0 \ (\text{if } V(x_{rel}) \leq \epsilon), \\ & \quad A_k q_k + B_k^- u_k + B_k^+ u_{k+1} + c_k = q_{k+1}, \\ & \quad H_k \begin{bmatrix} U_{y,k} \\ r_k \end{bmatrix} - G_k \leq \begin{bmatrix} \sigma_{\beta,k} \\ \sigma_{r,k} \end{bmatrix}, \\ & \quad M_{HJI} u_j + b_{HJI} \geq -\sigma_{HJI} \ (\text{if } V(x_{rel}) \leq \epsilon), \\ & \quad \text{for } j = 1, \dots, N_{HJI}, \quad k = 1, \dots, N. \end{aligned} \quad (10)$$

The objective strives to minimize a combination of tracking error (longitudinal, lateral and angular), control

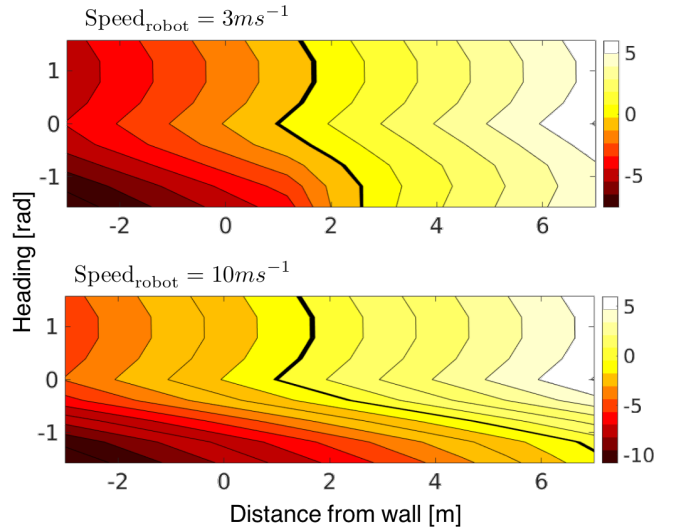


Figure 7. The BRS of the robot-wall system where zero heading corresponds to the robot car being parallel to the wall.

rates (steering and longitudinal tire forces), and magnitude of the slack variables. The constraints ensure (i) continuity with the current and next state and control, (ii) the change in controls across each time step is bounded, (iii) the positivity of slack variables, (iv) the (linearized) dynamics are satisfied, (v) the vehicle stability constraints are satisfied, and (vi) the HJI safety-preserving half-plane constraint is satisfied when $V(x_{rel}) \leq \epsilon$.

The time-discretization and linearizations (dynamics and constraints) we apply amount to an approximate variant of sequential quadratic programming (SQP). In particular, however, we solve one QP at each MPC step rather than the usual iteration until convergence. Since the tracking problems are so similar from one MPC step to the next, we find that this approach yields sufficient performance for our purposes. We interpolate along each solution trajectory to compute the linearization nodes for the QP at the next MPC step.

We use the `ForwardDiff.jl` automatic differentiation (AD) package implemented in the Julia programming language (Revels et al. 2016) to linearize the trajectory tracking dynamics as well as the HJI relative dynamics for the safety-preserving constraint. We call the Operator Splitting Quadratic Program (OSQP) solver (Stellato et al. 2017) through the `Parametron.jl` modeling framework (Koolen and contributors 2018); this combination of software enables us to solve the following MPC optimization problem at 100Hz. The MPC code, including optimization parameters and vehicle parameters (also included in Appendix A and B), can be found here: <https://github.com/StanfordASL/Pigeon.jl>.

6.2 Adding Static Obstacles

The current formulation does not prevent the robot from driving very far from its nominal trajectory (e.g., completely off the road) in order to avoid the human. In more realistic road settings, there could be environmental constraints such as a concrete road boundary. In the same way that collision avoidance with a human-controlled vehicle is formulated as

an additional constraint to the robot's MPC problem, we can add another safety constraint to account for a static wall to prevent the robot from swerving completely off the road. We consider two approaches for deriving this constraint: the first based on an additional HJI computation and giving rise to a similar control constraint applied over the first N_{HJI} timesteps, and the second treating the wall as a static obstacle with associated state constraints that apply over the whole duration of the MPC trajectory optimization.

For the first approach, we can compute a value function $V_{\text{WALL}}(x_{\text{R}})$ describing the interaction between the robot and the wall by using Equation (5) without the $p_{x_{\text{R}}}$ state (we only care about the distance from the wall and not how far along the wall the robot is). Two slices of the robot-wall BRS projected on the $p_{y_{\text{R}}} - \psi_{\text{R}}$ plane are illustrated in Figure 7. Intuitively, if the robot is moving towards the wall, the faster it is moving, the further away it needs to be away from the wall in order for there to exist an optimal collision avoidance control. Note that since the wall is static, there is no disturbance input. The robot-wall HJI control constraint $M_{\text{WALL}} u_{\text{R}} + b_{\text{WALL}} \geq 0$ becomes active when $V_{\text{WALL}}(x_{\text{R}}) \leq \epsilon$. This means that it is possible for both HJI-safety constraints to be active simultaneously. We note that theoretically we could consider the robot, human, and wall simultaneously by computing the BRS for the joint system. However, naively increasing the state size without any decomposition would be computationally undesirable even offline. Thus we treat the human-robot and robot-wall systems separately, but will discuss later the impact of this design choice.

Alternatively, we can account for a static wall by adding lateral error bound constraints into the MPC tracking problem—this is the approach taken in Brown et al. (2017). This involves always adding a left and right lateral error constraint ($e_{\min,k} \leq e_k \leq e_{\max,k}$) on each node point along the MPC trajectory such that the lateral deviation from the desired trajectory does not exceed the lateral distance to the wall. Specifically, we add the following constraints to the QP in Equation (10):

$$e_k - e_{k,\min} \geq -\sigma_e, \quad e_{k,\max} - e_k \geq -\sigma_e \quad \text{for } k = 1, \dots, N$$

as well as a slack penalty, $W_e \sigma_e$ to the cost function. This approach ensures no collision with the wall over the MPC time horizon only (in contrast to HJI which is over an infinite time horizon) and in general provides higher tracking performance because the MPC controller can optimize tracking states and controls over the entire tracking trajectory. We investigate both these approaches and provide more discussion in Section 8.

6.3 BRS Computation

We use the BEACLS toolkit (Tanabe and Chen 2018) implemented in C++ to compute the BRS. Since HJ reachability suffers from the curse of dimensionality, this is, to the best of our knowledge, the first attempt to use HJ reachability to compute the BRS for a seven-state relative system, especially with such high modeling fidelity. We, however, do sacrifice on grid size and use a relatively coarse grid compared to other literature standards. We linearly interpolate between grid points in order to evaluate the



Figure 8. X1: a steer-by-wire experimental vehicle platform. The 1/10-scale RC car has a mast that is visible to the LiDARs.

value function and its gradient at any given state (human-robot relative state or robot-wall state). We use a grid size of $13 \times 13 \times 9 \times 9 \times 9 \times 9 \times 9$ for our 7D system uniformly spaced over $(p_{x_{\text{rel}}}, p_{y_{\text{rel}}}, \psi_{\text{rel}}, U_{x_{\text{R}}}, U_{y_{\text{R}}}, v_{\text{H}}, r_{\text{R}}) \in [-15, 15] \times [-5, 5] \times [-\pi/2, \pi/2] \times [1, 12] \times [-2, 2] \times [1, 12] \times [-1, 1]$; computing the BRS with this system and discretization takes approximately 70 hours on a 3.0GHz octocore AMD Ryzen 1700 CPU.

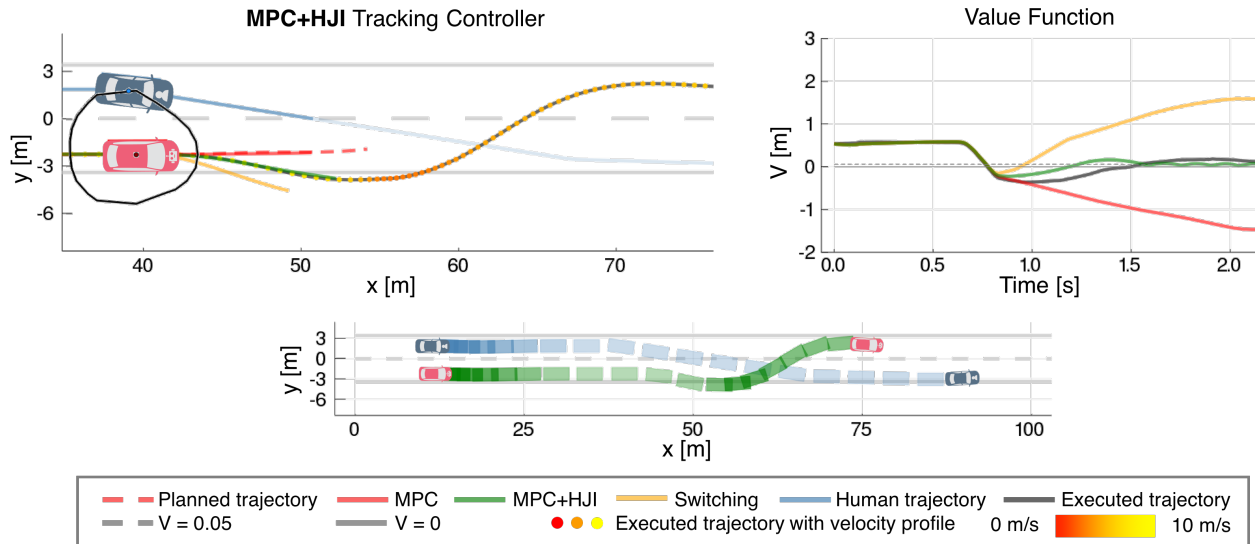
Computing the BRS requires computing the optimal control and disturbance defined in Equation (2). For the relative dynamics model, the optimal disturbance (i.e., human actions) is a bang-bang solution since the disturbance is affine. Due to the highly nonlinear nature of the dynamics, we use a uniform grid search across δ and F_x to calculate optimal actions (i.e., robot actions).

For the robot-wall system, we compute the optimal control actions in the same fashion. We use a grid size of $21 \times 9 \times 9 \times 9 \times 9$ uniformly spaced over $(p_{y_{\text{R}}}, \psi_{\text{R}}, U_{x_{\text{R}}}, U_{y_{\text{R}}}, r_{\text{R}}) \in [-3, 7] \times [-\pi/2, \pi/2] \times [1, 12] \times [-2, 2] \times [-1, 1]$; computing the BRS with this system and discretization takes approximately 40 minutes.

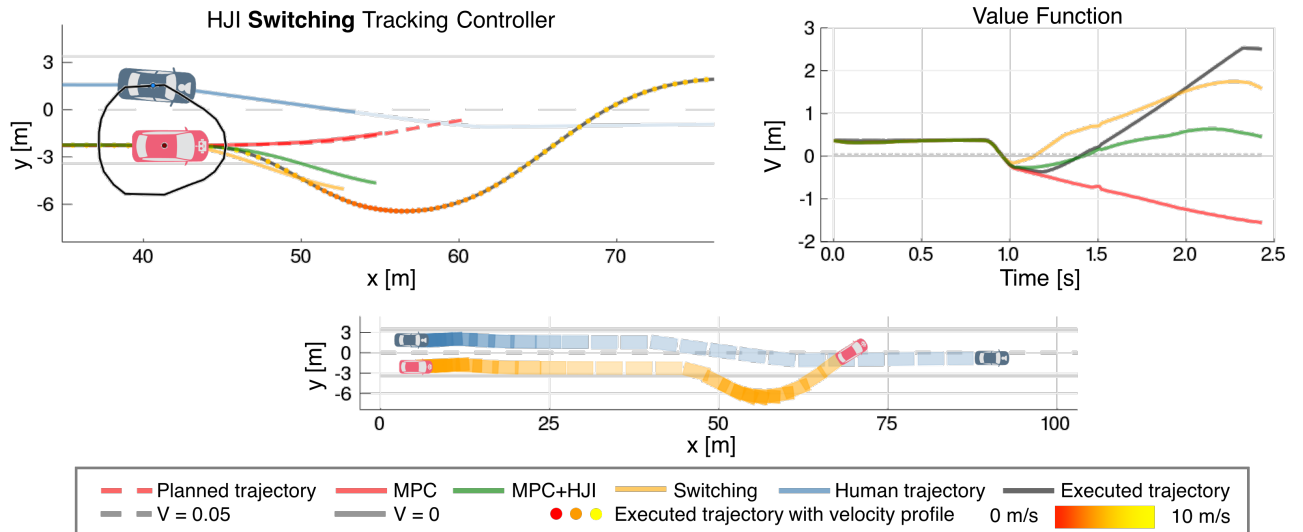
7 Results

7.1 Experimental Vehicle Platform

X1 is a flexible steer-by-wire, drive-by-wire, and brake-by-wire experimental vehicle developed by the Stanford Dynamic Design Lab (see Figure 8). It is equipped with three LiDARs (one 32-beam and two 16-beam), a differential GPS/INS which provides 100Hz pose estimates accurate to within a few centimeters as well as high fidelity velocity, acceleration, and yaw rate estimates. To control X1, desired steering (δ) and longitudinal tire force (F_{x_f}, F_{x_r}) commands are sent to the dSpace MicroAutoBox (MAB) which handles all sensor inputs except LiDAR (handled by the onboard PC) and implements all low level actuator controllers. Similarly, state information about the vehicle is obtained from the MAB. We use the Robot Operating System (ROS) to communicate with the MAB which handles sensing and control at the hardware level; the planning/control stack described in this work is running onboard X1 on a consumer desktop PC running Ubuntu 16.04 equipped with a quadcore Intel Core i7-6700K CPU and an NVIDIA GeForce GTX 1080 GPU. X1 parameters used in the equations of motion (Equation (5)) are listed in Appendix A.



(a) Controller comparison on experimental data where the robot car uses the MPC+HJI controller.



(b) Controller comparison on experimental data where the robot car uses the switching controller.

Figure 9. Controller comparison on planner trajectories from X1-virtual human-driven vehicle experiments. Left: Simulations of using the MPC, MPC+HJI, and switching controllers when $V(x_{\text{rel}}(t))$ first drops below $\epsilon = 0.05$ are shown, and are compared against the executed trajectory (from experiments) and the desired trajectory (from the interaction planner). Right: The corresponding evolutions of $V(x_{\text{rel}}(t))$. Bottom: Illustration of the traffic-weaving interaction. The human controlled car (blue car) carelessly drives into the path of the robot car (red car), causing the robot car to react by swerving. The transparency of the rectangles corresponds to the speed of the car (higher transparency corresponds to higher speed).

We also perform experiments using a LiDAR-visible 1/10-scale RC car (Figure 8 right) as the human-driven car to investigate the robustness of our proposed control stack with perception uncertainty.

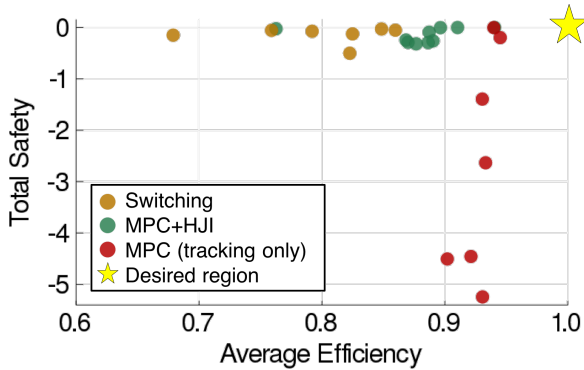
The code used to run the experiments can be found here: https://github.com/StanfordASL/safe_traffic_weaving.

7.2 Experiments

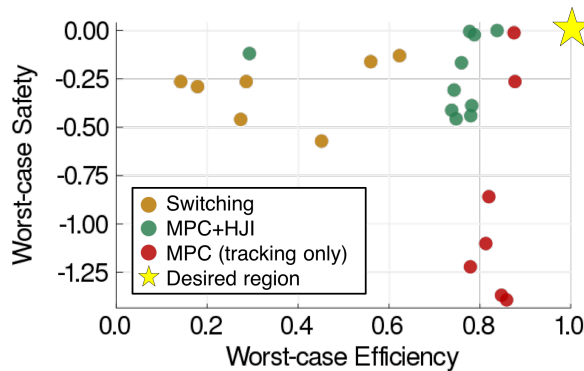
To evaluate our proposed control stack—a synthesis of a high-level probabilistic interaction planner with the MPC+HJI tracking controller—we perform full-scale human-in-the-loop traffic-weaving trials with X1 taking on the role of the robot car. To ramp up towards testing with two full-scale vehicles in the near future, we investigate two

types of human car: (i) a virtual human-driven car and (ii) a 1/10-scale LiDAR-visible human-driven RC car. We scale the highway traffic-weaving scenario (mean speed ~ 28 m/s) in Schmerling et al. (2018) down to a mean speed of ~ 8 m/s by shortening the track (reducing longitudinal velocity by a constant) and scaling time by a factor of 4/3 (with the effect of scaling speeds by 3/4 and accelerations by 9/16). The value of the parameters in the MPC tracking problem are listed in Appendix B.

We investigate and evaluate the effectiveness of our control stack by allowing the human car to act carelessly (i.e., swerving blindly towards the robot car) during the experiments. In Sections 7.2.1 and 7.2.2 we compare our proposed controller (MPC+HJI) against a tracking-only MPC controller (MPC) and a controller that switches to the



(a) Trade-off between total safety and average efficiency.



(b) Trade-off between worst-case safety and worst-case efficiency.

Figure 10. Safety and efficiency trade-offs for the different control strategies.

HJI optimal avoidance controller when near safety violation (switching). In Section 7.2.3 we compare the two static obstacle avoidance approaches developed in Section 6.2 to a scenario with a virtual wall constraining the robot’s trajectory. We investigate applying an extension of the same state-constraint-based static obstacle avoidance strategy to the problem of collision with a dynamic obstacle (the human) in Section 7.2.4 and discuss its shortcomings. Finally, in Section 7.2.5 we present experiments with the human car physically embodied by an RC car.

7.2.1 Virtual Human-Driven Vehicle To ensure a completely safe experimental environment, our first tier of experimentation uses a joystick-controlled virtual vehicle for the human car and allows the robot control stack to have perfect observation of the human car state. Experimental trials of the probabilistic planning framework using (i) our proposed approach (MPC+HJI) and (ii) switching to the optimal HJI controller (switching) are shown in Figure 9, along with a simulated comparison between the two safety controllers and the tracking-only controller (MPC). For comparative purposes, the controllers were simulated with the displayed nominal trajectory held fixed, but in reality, the nominal trajectory in these experiments was updated at $\sim 3\text{Hz}$. As expected, we see that when safety violation occurs, the MPC+HJI controller represents a middle ground between the tracking-only MPC which does not react to the human car’s intrusion, and the switching controller which arguably overreacts with a large excursion outside the lane boundaries. Evidently, our proposed controller tries to be minimally

interventional—the robot car swerves/brakes but only to an extent that is necessary.

Looking at the value function, we see that, as expected, the MPC+HJI controller aims to keep the value positive, but does not necessarily strive to increase it, while the switching controller aims to increase the value as much as possible. The MPC (tracking only) controller fails to increase the value at all when safety violation occurs. All controllers however, experience a period where the value is negative, even the two HJI-based controllers which theoretically guarantee safety. We believe this is due to model mismatch; we will discuss this point in more depth in Section 8.

Additionally, in some trials when the robot car was traveling faster, the activation of the HJI constraint resulted in the robot car performing a large but smooth swerve that traversed completely outside the lane boundaries. We address this limitation by adding a wall constraint into the MPC formulation discussed in Section 7.2.3.

7.2.2 Safety and Efficiency Trade-off Our MPC+HJI controller considers the set of safety-preserving controls while optimizing its tracking performance when it is near safety violation. In contrast, the HJI switching controller uses the optimal avoidance control policy and as a result neglects to track the desired trajectory that was selected by the planner for interaction performance. As such, there is a trade off between safety, defined with respect to the value function, and efficiency.

For use as a comparison metric, we define the notion of *total safety* of an interaction of time length T as

$$S_{\text{total}} := \int_0^T \mathbf{1}[V(x_{\text{rel}}(t)) \leq 0] V(x_{\text{rel}}(t)) dt$$

which is the integral of the value function when it is negative. Total safety considers not only the magnitude of the safety violation, but also the duration of the violation. We can also define the *worst-case safety* as

$$S_{\text{worst}} := \min_{t \in [0, T]} V(x_{\text{rel}}(t))$$

which does not consider the duration of safety violation, but rather the worst-case safety violation with respect to the value function over the interaction.

Efficiency of the interaction is more difficult to quantify. In this analysis, we define efficiency with respect to the *g-forces* experienced by the vehicle as this is a proxy for control effort and passenger comfort. Alternative metrics include time taken to complete the interaction, and friction available in the tires. We define *average efficiency* as

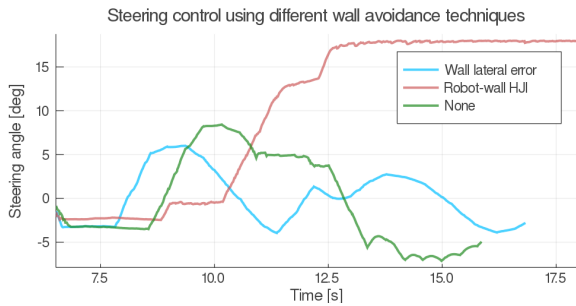
$$E_{\text{avg}} := 1 - \frac{1}{T} \int_0^T \frac{1}{g} \sqrt{a_x(t)^2 + a_y(t)^2} dt$$

where $a_x(t)$ and $a_y(t)$ are the x and y acceleration of the robot car; larger E_{avg} values correspond to better efficiency. *g-forces* should not exceed one as this is beyond the physical limits of a vehicle. We also define the *worst-case efficiency* as

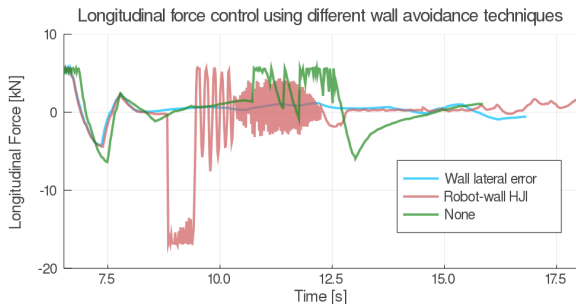
$$E_{\text{worst}} := \max_{t \in [0, T]} \left(1 - \frac{1}{g} \sqrt{a_x(t)^2 + a_y(t)^2} \right)$$

which considers the largest *g-force* experienced during the interaction.

Given these quantities, we can compare the safety and efficiency trade-offs between the MPC, MPC+HJI, and switching controllers. Multiple experimental trials using X1 were carried out using each controller, and Figure 10a compares the average/total metrics while Figure 10b compares the worst-case metrics. We see that in both cases, the MPC+HJI controller provides a good balance between safety and efficiency; the safety almost equaling that of the optimal switching controller, and efficiency almost equaling that of the MPC controller. The switching controller provides the highest level of safety (with respect to the value function) but experiences lower efficiency since it often results in heavy braking and sharp swerving. The MPC controller provides lower safety scores but with larger variations as the resulting safety score is scenario dependent rather than controller dependent.



(a) Comparison of steering angle. The plot begins when the robot car is planning autonomously.



(b) Comparison of longitudinal force. The plot begins when the robot car is planning autonomously.

Figure 11. Comparison of control sequences from using MPC lateral error state constraints, robot-wall HJI control constraint, and no constraints to avoid a static road boundary.

7.2.3 Static wall We investigate two methods, (i) persistently adding lateral error state constraints into the MPC problem and (ii) adding an additional HJI-based control constraint for a robot-wall relative system into the MPC problem when $V_{\text{WALL}}(x_R) \leq \epsilon$, for avoiding a static (virtual) road boundary wall when the robot car is swerving off the road to avoid a collision with the human car.

Figure 11 compares the control sequences and Figure 12 compares the trajectory of both approaches. Here, the human car is commanded to stay in the lane and is initialized inside the BRS so that when the robot starts planning autonomously, the robot car will react immediately and swerve out of the way—we investigate the nature of the swerving. We do note that the human car is able to make the robot car swerve even though it is staying in its lane. This is due to the wide, pear-shape BRS when the two cars are

parallel and at similar speeds (see Figure 1b left). We discuss this in more detail in Section 8.

Around 20 meters from the start of the roadway in Figure 12, the robot car begins to plan autonomously. Before then, the cars are following a straight line in order to speed up from $\approx 1m/s$ to the desired interaction speed. To provide the cleanest comparison, all results in this subsection are derived from simulation. Starting in the right lane, we see in all cases that when safety is violated the robot car swerves to the right ($\delta < 0$). When using the lateral error constraints (Figure 12, top), the robot car essentially has a “look-ahead” capability because it is able to optimize its steering commands over the MPC tracking horizon, essentially distributing the responsibility of avoiding the wall across the entire tracking MPC horizon. As a result, the robot car is able to successfully and smoothly steer back onto the road and avoid the wall.

When using the robot-wall HJI control constraint (Figure 12, center), the robot car does not preemptively swerve back onto the road and instead only reacts to the wall when $V_{\text{WALL}}(x_R) \leq \epsilon$ as designed. The robot car performs a hard brake to the point of almost stopping[§] and then begins to eventually command a maximum steering angle (18 deg). The sharp and abrupt behavior stems from the HJI formulation assuming the robot can and will take extreme actions, including cases when using the safety-preserving control set. As a result, the responsibility for evasive action is triggered at the very latest possible instance and compressed into a control constraint over a single (in practice 3) MPC timestep. This is in contrast to the other approach of always having MPC lateral error state constraints over the entire MPC horizon. The MPC+HJI controller is effective in avoiding dynamic obstacles, but for static obstacles, HJI is not suitable because it is unnecessary to reason about the dynamics of something that is static. With no wall constraints (Figure 12, bottom), the robot car swerves completely off the road, and in order to quickly get to the left lane before the end of the road (inscribed as an objective in the high-level planner), it overshoots to the other side of the road and also drives beyond the road boundary on the other side.

7.2.4 Comparison to baseline dynamic obstacle avoidance Motivated by the success of applying state constraints in the previous section, we compare our proposed framework (MPC+HJI for safe human-robot interaction) with a baseline approach of avoiding collision with the human car using lateral error constraints. In order to define safety state constraints over the duration of the robot trajectory, we must however make some assumption on the human’s future trajectory. For this baseline, at each MPC iteration, we assume that the human car will continue moving at its current heading and with its current velocity.[¶] The lateral error constraint at each MPC time step is computed between

[§]Since the dynamic bicycle model is ill-defined for low speeds (thus explaining the oscillations in F_x), the experiment (when using the robot-wall HJI control constraint) is essentially over around $t = 9$. In general, the MPC problem can switch to the kinematic model at low speeds (Patterson et al. 2018) which is well defined in that speed region.

[¶]Alternatively, one could use a sample or a *maximum a posteriori* estimate from the interaction planner’s prediction model.

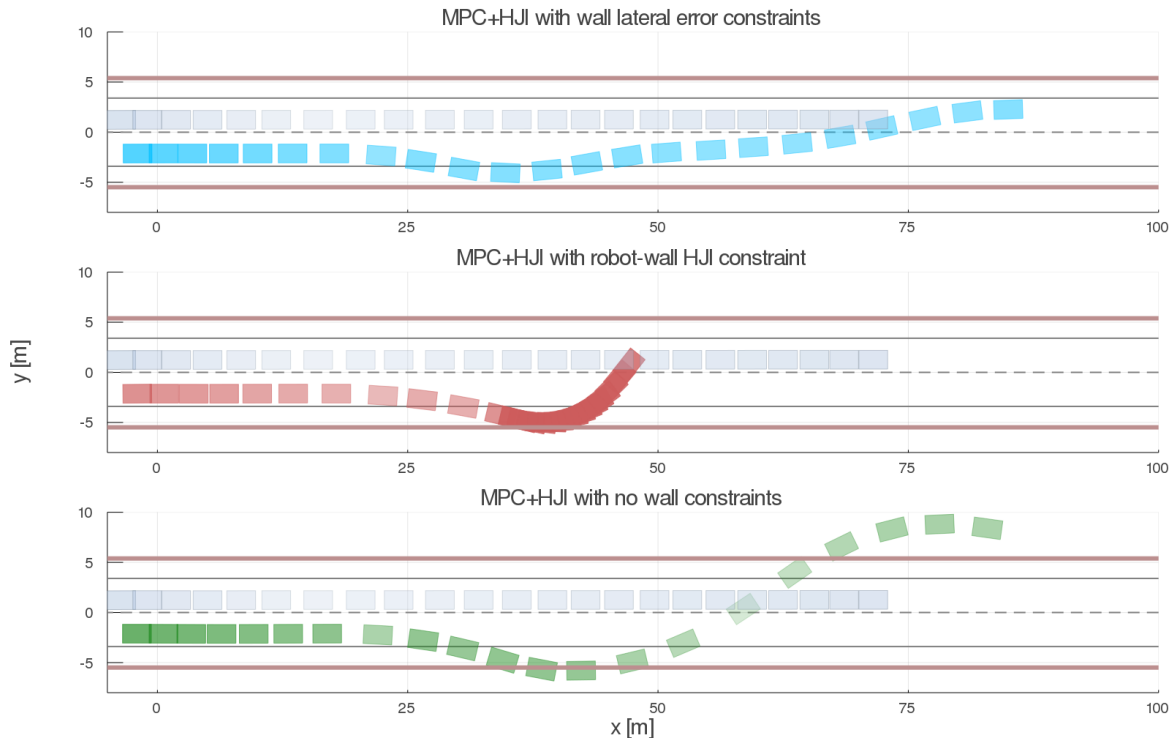


Figure 12. Trajectory comparison between using lateral error constraints (top), a robot-wall HJI control constraint (middle), and using no wall constraints (bottom). The human car is in the left (top) lane and is constant across all three trials, and the robot car is in the right (bottom) lane. The transparency of the car corresponds to the speed of the car (higher transparency corresponds to higher speed).

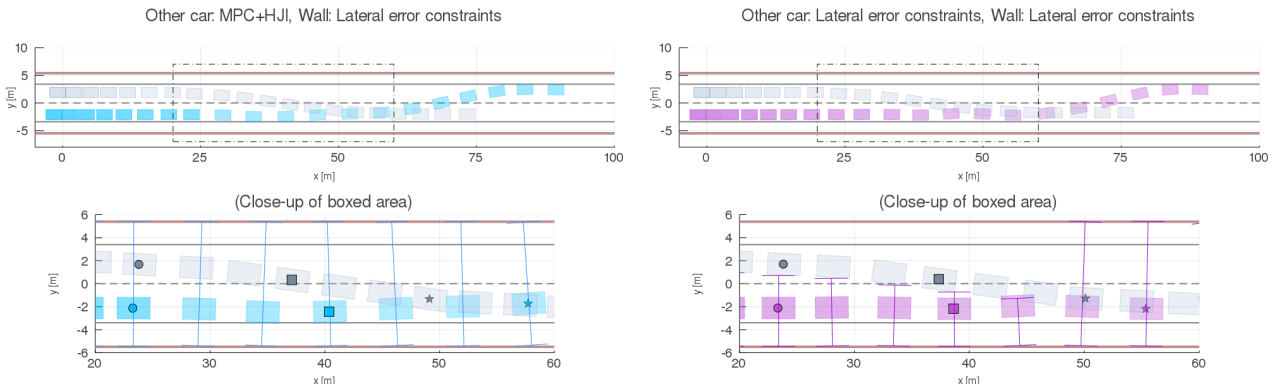


Figure 13. Comparison between the MPC+HJI controller (left) and a baseline approach not based on any reachability analysis (right) for the task of dynamic obstacle avoidance. The trajectory of the human car starting in the left (top) lane is visualized in gray; the trajectory of the robot car starting in the right (bottom) lane is visualized in color. In each close-up view, error bars accompanying each snapshot of the robot illustrate the first ($k = 1$) lateral state constraint of the MPC problem at that step. To help correspond the positions of the cars over the trials, each pair of matching-shape markers represents a common time instant.

the robot's desired trajectory and the human's projected trajectory—this is analogous to applying the approach taken in Brown et al. (2017) but with (deterministic) dynamic obstacles. A simulation of our proposed approach and the baseline approach is shown in Figure 13. Notably, in this simulation, the human car defies the baseline's linear-extrapolation-based prediction model and curves into the other lane towards the robot car.

We see in Figure 13a that when using the MPC+HJI controller (with lateral error state constraints for wall avoidance), we are able to successfully avoid a collision with

the human car and the wall, and maintain relative states outside the BRS. The baseline approach demonstrated in Figure 13b, on the other hand, collides with the human because its consideration of only one possible future (i.e., human trajectory) at each MPC step leads the robot into a region of inevitable collision (defined against all, including worst-case, human controls). In particular we see that as the human trajectory increases its curvature towards the middle of the lane change, the lateral error bounds (based on an assumption of constant velocity) are not stringent enough to maintain robot safety. The utility of the MPC+HJI approach

is that it distills safety considerations with respect to all possible realizations of the human trajectory into a single control constraint. Moreover, this constraint is not overly conservative (to improve the state-constraint-based approach one might imagine defining lateral error constraints to avoid the entire forward reachable set of the human), because it incorporates the concept of closed-loop feedback into its BRS computation.

7.2.5 1/10-Scale Human-Driven Vehicle To begin investigating the effects of perception uncertainty on our safety assurance framework, we use three LiDARs onboard X1 to track a human-driven RC car, and implement a Kalman filter for human car state estimation (position, velocity, and acceleration). Even with imperfect observations, we show some successful preliminary results (an example is shown in Figure 14) at mean speeds of 4m/s, close to the limits of the RC car + LiDAR-visible mast in crosswinds at the test track. We observe similar behavior as in the virtual human car experiments, including the fact that the value function dips briefly below zero before the MPC+HJI controller is able to arrest its fall; we discuss this behavior in the next section.

8 Discussion

Beyond the qualitative and quantitative confirmation of our design goals, our experimental results reveal three main insights.

Takeaway 1: The reachability cache is underly-conservative with respect to robot car dynamics and overly-conservative with respect to human car dynamics.

In all cases—hardware experiments as well as simulation results—the HJI value function V dips below zero, indicating that neither the HJI+MPC nor even the optimal avoidance switching controller are capable of guaranteeing safety in the strictest sense. The root of this apparent paradox is in the computation of the reachability cache used by both controllers as the basis of their safety assurance. Though the 7-state relative dynamics model (Equation (8)) subsumes a single-track vehicle model that has proven successful in predicting the evolution of highly dynamic vehicle maneuvers (Funke et al. 2017; Brown et al. 2017), the way it is employed in computing the value function V omits relevant components of the dynamics. In particular, when computing the optimal avoidance control (Equation (2)) as part of solving the HJI PDE, we assume total freedom over the choice of robot steering angle δ and longitudinal force command F_x , up to maximum control limits. This does not account for, e.g., limits on the steering slew rate (traversing $[\delta_{\min}, \delta_{\max}]$ takes approximately 1 second), and thus the value function is computed under the assumption that the robot can brake/swerve far faster than it actually can.

We note that simply tuning the safety buffer ϵ is insufficient to account for these unmodeled dynamics. In Figure 9a we see that V may drop from approximately 0.5 (the value when the two cars traveling at 8m/s start side-by-side in lanes) to -0.3 in the span of a few tenths of a second. Selecting $\epsilon > 0.5$ might give enough time for the steering to catch up, but such a selection would prevent the robot car from accomplishing the traffic weaving task

even under nominal conditions, i.e., when the human car is equally concerned about collision avoidance. Even for $\epsilon = 0.05$, we see that the human car can cause the robot to swerve by just staying its lane but with a small offset towards the robot’s lane (see Figure 12). This is because the safety controller would push the robot car outside of its lane from the outset to maintain the buffer. This behavior follows from wide level sets associated with the transient control authority asymmetry (recall that in the HJI relative dynamics the human car may adjust its trajectory curvature discontinuously), assumed as a conservative safety measure as well as a way to keep the relative state dimension manageable.

The simplest remedy for both of these issues is to increase the fidelity of the relative dynamics model by incorporating additional integrator states $\dot{\delta}$ for the robot and $\dot{\omega}$ for the human. Naively increasing the state dimension to 8 or 9, however, might not be computationally feasible (even offline) without devising more efficient HJI solution techniques or choosing an extremely coarse discretization over the additional states. By literature standards we already use a relatively coarse discretization grid for solving the HJI PDE; associated numerical inaccuracies may be another source of the observed safety mismatch. We believe that simulation, accounting for slew rates, could be a good tool to prototype such efforts, noting that as it stands we have relatively good agreement between simulation and the experimental platform in our testing.

Takeaway 2: Interpretability of the value function V should be a key consideration in future work.

In this work the terminal value function $V(0, x_{\text{rel}})$ is specified as the separation/penetration distance between the bounding boxes of the two vehicles, a purely geometric quantity dependent only on $p_{x,\text{rel}}$, $p_{y,\text{rel}}$, and ψ_{rel} . Recalling that V ($:= V_\infty$) represents the worst-case eventual outcome of a differential game assuming optimal actions from both robot and human, we may interpret the above results through the lens of worst-case outcomes, i.e., a value of -0.3 may be thought of as 30cm of collision penetration assuming optimal collision seeking/avoidance from human/robot. When extending this work to cases with environmental obstacles (e.g., concrete highway boundaries that preclude large deviations from the lane), or multi-agent settings where the robot must account for the uncertainty in multiple other parties’ actions, for many common scenarios it may be the case that guaranteeing absolute safety is impossible. Instead of avoiding a BRS of states that might lead to collision, we should instead treat the value function inside the BRS as a cost. In particular we should specify more contextually relevant values of $V(0, x_{\text{rel}})$ for states in collision, e.g., negative kinetic energy or another notion of collision severity as a function of the velocity states $U_{x,\text{R}}$, $U_{y,\text{R}}$, v_{H} , and r_{R} in addition to the relative pose. This would lead to a controller that prefers, in the worst case, collisions at lower speed, or perhaps “glancing blows” where the velocities of the two cars are similar in magnitude and direction.

Takeaway 3: Static obstacles should be accounted for using MPC tracking state constraints and not HJI control constraints. It is natural to use HJI when reasoning about potential dangers from a dynamic, unpredictable agent,

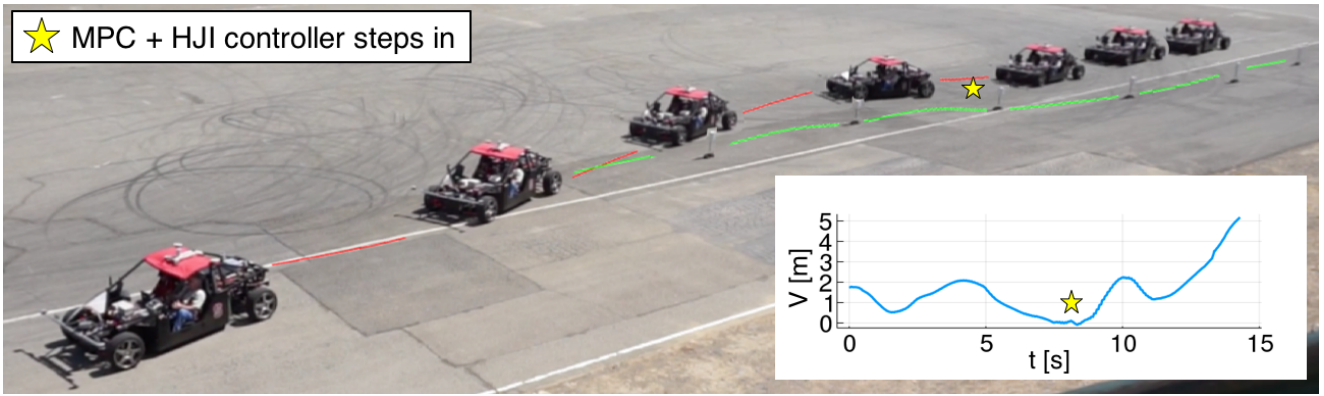


Figure 14. Time-lapse of pairwise vehicle interaction: X1 with 1/10-scale human-driven RC car. The RC car (green trajectory) nudges into X1 (red trajectory), which swerves gently to avoid. Inset: The value function over time of the X1-human driven RC car experiment

but for static obstacles there is no uncertainty in how the obstacle may act. That is, when the other agent is deterministic, there is no notion of optimizing robot safety policies over all worst-case actions by the other agent. Indeed, in this case it is possible to confidently extend the safety constraint along the entire MPC horizon, as demonstrated in Section 7.2.3. This is as opposed to deriving a safety constraint to be applied at the first step (on the present control action; the HJI+MPC approach), as must be done with a nondeterministic agent with unknown future trajectory. Spreading the collision avoidance constraint over the problem horizon allows for the MPC optimization to more smoothly accomplish its objectives (i.e., control smoothness and tracking performance) while maintaining safety. We note, however, that naive extensions of this approach to nondeterministic agents (recall Section 7.2.4) do not similarly provide strong safety assurances.

9 Conclusions

We have investigated a control scheme for providing real-time safety assurance to underpin the guidance of a probabilistic planner for human-robot vehicle-vehicle interactions. By essentially projecting the planner’s desired trajectory into the set of safety-preserving controls whenever safety is threatened, we preserve more of the planner’s intent than would be achieved by adopting the optimal control with respect to separation distance. Our experiments show that with our proposed minimally interventional safety controller, we accomplish the high level objective (traffic weaving) despite the human car swerving directly onto the path of the robot car, and accomplish this relatively smoothly compared to using a switching controller that results in the robot car swerving more violently off the road. Further, we investigate the addition of a road boundary wall to our formulation to prevent the robot car from swerving completely out of the lane which could be dangerous in realistic road settings, and compare against a baseline approach using state constraints to avoid dynamic obstacles to show that our framework is better designed to keep the robot car safe even in the face of worst-case human car behaviors.

We note that this work represents only a promising first step towards the integration of reachability-based safety guarantees into a probabilistic planning framework. Future

work includes investigating this framework for cases where the human and robot have very different dynamics, such as a pedestrian or cyclist interacting with a car, or a human interacting with a robotic manipulator, and for interactions involving multiple (more than two) agents. We may also consider adapting our approach to ensure high planning performance while guaranteeing satisfaction of constraints other than safety, e.g., task requirements specified by temporal logic constraints as considered in Chen et al. (2018). In the context of human-robot vehicle interactions, we have already discussed the concrete modifications to this controller we believe are necessary to improve the practical impact of our theoretical guarantees; further study should also consider better fitting of the planning objective at the controller level. That is, instead of performing a naive projection, i.e., the one that minimizes trajectory tracking error, it is likely that a more nuanced selection informed by the planner’s prediction model would represent a better “backup choice” in the case that safety is threatened. We recognize that ultimately, guaranteeing absolute safety on a crowded roadway may not be realistic, but we believe that in such situations value functions derived from reachability may provide a useful metric for near-instantly evaluating the future implications of a present action choice.

Acknowledgements

This work was supported by the Office of Naval Research (Grant N00014-17-1-2433), by Qualcomm, and by the Toyota Research Institute (“TRI”). This article solely reflects the opinions and conclusions of its authors and not ONR, Qualcomm, TRI, or any other Toyota entity. The authors would like to thank the X1 team, in particular Matt Brown, Larry Cathey, and Amine Elhafsi, Matteo Zallio, and the Thunderhill Raceway Park for accommodating testing.

References

- Althoff M and Dolan J (2014) Online verification of automated road vehicles using reachability analysis. *IEEE Transactions on Robotics* 30(4): 903–918.
- Althoff M and Dolan JM (2011) Set-based computation of vehicle behaviors for the online verification of autonomous vehicles. In: *Proc. IEEE Int. Conf. on Intelligent Transportation Systems*.

- Althoff M and Krogh BH (2014) Reachability analysis of nonlinear differential-algebraic systems. *IEEE Transactions on Automatic Control* 59(2): 371–383.
- Arora S, Choudhury S, Althoff D and Scherer S (2015) Emergency maneuver library – ensuring safe navigation in partially known environments. In: *Proc. IEEE Conf. on Robotics and Automation*.
- Bajcsy A, Bansal S, Bronstein E, Tolani V and Tomlin CJ (2019) An efficient reachability-based framework for provably safe autonomous navigation in unknown environments. In: *Proc. IEEE Conf. on Decision and Control*.
- Bokanowski O, Forcadel N and Zidani H (2010) Reachability and minimal times for state constrained nonlinear problems without any controllability assumption. *SIAM Journal on Control and Optimization* 48(7): 4292–4316.
- Brown M, Funke J, Erlien S and Gerdès JC (2017) Safe driving envelopes for path tracking in autonomous vehicles. *Control Engineering Practice* 61: 307–316.
- Chen M, Hu Q, Fisac J, Akametalu K, Mackin C and Tomlin C (2017) Reachability-based safety and goal satisfaction of unmanned aerial platoons on air highways. *AIAA Journal of Guidance, Control, and Dynamics* 40(6): 1360 – 1373.
- Chen M, Tam Q, Livingston SC and Pavone M (2018) Signal temporal logic meets Hamilton-Jacobi reachability: Connections and applications. In: *Workshop on Algorithmic Foundations of Robotics*. In Press.
- Chen M and Tomlin CJ (2018) Hamilton–Jacobi reachability: Some recent theoretical advances and applications in unmanned airspace management. *Annual Review of Control, Robotics, and Autonomous Systems* 1(1): 333–358. DOI:10.1146/annurev-control-060117-104941.
- Dhinakaran A, Chen M, Chou G, Shih JC and Tomlin CJ (2017) A hybrid framework for multi-vehicle collision avoidance. In: *Proc. IEEE Conf. on Decision and Control*.
- Fisac JF, Akametalu AK, Zeilinger MN, Kaynama S, Gillula J and Tomlin CJ (2018) A general safety framework for learning-based control in uncertain robotic systems. *IEEE Transactions on Automatic Control* 64(7): 2737–2752.
- Fisac JF, Chen M, Tomlin CJ and Sastry SS (2015) Reach-avoid problems with time-varying dynamics, targets and constraints. In: *Hybrid Systems: Computation and Control*.
- Frehse G, Le Guernic C, Donzé A, Cotton S, Ray R, Lebeltel O, Ripado R, Girard A, Dang T and Maler O (2011) Spaceex: Scalable verification of hybrid systems. In: *Proc. Int. Conf. Computer Aided Verification*.
- Funke J, Brown M, Erlien SM and Gerdès JC (2017) Collision avoidance and stabilization for autonomous vehicles in emergency scenarios. *IEEE Transactions on Control Systems Technology* 25(4): 1204 – 1216.
- Gattami A, Al Alam A, Johansson KH and Tomlin CJ (2011) Establishing safety for heavy duty vehicle platooning: A game theoretical approach. *IFAC World Congress* 44(1): 3818–3823.
- Gray A, Gao Y, Hedrick JK and Borrelli F (2013) Robust predictive control for semi-autonomous vehicles with an uncertain driver model. In: *IEEE Intelligent Vehicles Symposium*.
- Greenstreet MR and Mitchell I (1998) Integrating projections. In: *Hybrid Systems: Computation and Control*.
- Koolen T and contributors (2018) Parametron.jl: Efficiently solving instances of a parameterized family of optimization problems in Julia. Available at <https://github.com/tkoolen/>
- Parametron.jl.
- Kurzhanski A and Varaiya P (2000) Ellipsoidal techniques for reachability analysis: Internal approximation. *System and Control Letters* 41(3): 201–211.
- Liu SB, Roehm H, Heinemann C, Ltkebohle I, Oehlerking J and Althoff M (2017) Provably safe motion of mobile robots in human environments. In: *IEEE/RSJ Int. Conf. on Intelligent Robots & Systems*.
- Lorenzetti J, Chen M, Landry B and Pavone M (2018) Reach-avoid games via mixed-integer second-order cone programming. In: *Proc. IEEE Conf. on Decision and Control*.
- Majumdar A, Vasudevan R, Tobenkin MM and Tedrake R (2014) Convex optimization of nonlinear feedback controllers via occupation measures. *Int. Journal of Robotics Research* 33(9): 1209–1230.
- Margellos K and Lygeros J (2011) Hamilton-Jacobi formulation for reach-avoid differential games. *IEEE Transactions on Automatic Control* 56(8): 1849–1861. DOI:10.1109/TAC.2011.2105730.
- Mattingley J and Boyd S (2012) CVXGEN: A code generator for embedded convex optimization. *Optimization and Engineering* 12(1): 1–27.
- Mitchell IM, Bayen AM and Tomlin CJ (2005) A time-dependent Hamilton-Jacobi formulation of reachable sets for continuous dynamic games. *IEEE Transactions on Automatic Control* 50(7): 947–957.
- Pacejka H (2002) *Tire and Vehicle Dynamics*. Elsevier.
- Patterson V, Thornton S and Gerdès JC (2018) Tire modeling to enable model predictive control of automated vehicles from standstill to the limits of handling. In: *Int. Symp. on Advanced Vehicle Control*.
- Revels J, Lubin M and Papamarkou T (2016) Forward-mode automatic differentiation in julia. Available at <https://arxiv.org/abs/1607.07892>.
- Sadigh D, Sastry S, Seshia SA and Dragan AD (2016) Planning for autonomous cars that leverage effects on human actions. In: *Robotics: Science and Systems*.
- Schmerling E, Leung K, Vollprecht W and Pavone M (2018) Multimodal probabilistic model-based planning for human-robot interaction. In: *Proc. IEEE Conf. on Robotics and Automation*.
- Stellato B, Banjac G, Goulart P, Bemporad A and Boyd S (2017) OSQP: An operator splitting solver for quadratic programs Available at <https://arxiv.org/abs/1711.08013>.
- Tanabe K and Chen M (2018) BEACLS: Berkeley Efficient API in C++ for Level Set methods. Available at <https://github.com/HJReachability/beacls>.
- Wolf MT and Burdick JW (2008) Artificial potential functions for highway driving with collision avoidance. In: *Proc. IEEE Conf. on Robotics and Automation*.
- Yoon S, Fern A, Givan R and Kambhampati S (2008) Probabilistic planning via determinization in hindsight. In: *Proc. AAAI Conf. on Artificial Intelligence*.

A Vehicle Parameters

X1 parameters relevant to defining the equations of motion in Equation (5).

Table 1. X1 parameters

Description	Value
Standard Earth gravity	9.80665ms^{-2}
Total mass	1964kg
Yaw moment of inertia (I_{zz})	2900 kgm^2
Vertical height of CG (h)	0.47m
Distance from CG to front axle (d_f)	1.4978m
Distance from CG to rear axle (d_r)	1.3722m
Front cornering stiffness (C_{α_f})	150kN/rad
Rear cornering stiffness (C_{α_r})	220kN/rad
Drag coefficient C_{d_0}	241N
Drag coefficient C_{d_1}	$25.1\text{Nm}^{-1}\text{s}$
Drag coefficient C_{d_2}	$0.0\text{Nm}^{-2}\text{s}^2$
Front wheel drive fraction ($F_x \geq 0$)	0
Rear wheel drive fraction ($F_x \geq 0$)	1
Front wheel brake fraction ($F_x < 0$)	0.6
Rear wheel brake fraction ($F_x < 0$)	0.4

B Trajectory Parameters

Parameter values relevant for the MPC tracking optimization in Equation (10).

Table 2. MPC tracking optimization parameters

Description	Value
$Q_{\Delta s}$	1.0m^{-2}
$Q_{\Delta \psi}$	1.0
Q_e	1.0m^{-2}
$R_{\Delta \delta}$	0.1
$R_{\Delta F_x}$	0.5N^{-2}
W_β	$\frac{900}{\pi}$
W_r	50.0s
W_{HJI}	500.0m^{-1}
W_e	500.0m^{-1}
δ_{\min}	$-18 \times \frac{\pi}{180}$
δ_{\max}	$18 \times \frac{\pi}{180}$
$\Delta \delta_{\min}$	$-0.344 \Delta t$
$\Delta \delta_{\max}$	$0.344 \Delta t$
$F_{x,\min}$	-16794N
$F_{x,\max}$	$\min(5600, \frac{75000}{U_x})\text{N}$
$U_{x,\min}$	1.0ms^{-1}
$U_{x,\max}$	15ms^{-1}
N_{long}	10
N_{short}	5
N_{HJI}	3
Δt_{long}	0.2s
Δt_{short}	0.01s
ϵ	0.05